PERGAMON

Journal of Structural Geology 24 (2002) 1507–1520

JOURNAL OF STRUCTURAL GEOLOGY

www.elsevier.com/locate/jstrugeo

Magnetic fabric and petrographic investigation of hematite-bearing sandstones within ramp-related folds: examples from the South Atlas Front (Morocco)

B. Saint-Bezar[a,1,*], R.L. Hebert[b], C. Aubourg[b], P. Robion[b], R. Swennen[c], D. Frizon de Lamotte[b]

[a]*Département des Sciences de la Terre, UMR 8616 - CNRS ORSAYTERRE, Batiment 504, Universite de Paris-Sud, 91405-ORSAY Cedex, France*
[b]*Département des Sciences de la Terre, Université de Cergy Pontoise. CNRS-UMR 7072, 8 Le Campus, 95031 Cergy Cedex, France*
[c]*Katholieke Universiteit Leuven, Afdeling Fysico-chemische Geologie, Laboratorium voor Mineralogie, Celestijnenlaan 200C, 3001 Heverlee, Belgium*

Received 22 February 2001; revised 2 October 2001; accepted 23 October 2001

Abstract

An investigation of the anisotropy of magnetic susceptibility (AMS) of hematite-bearing sandstones has been carried out along two fault-propagation folds located at the front of the High Atlas Belt (Goulmima area, Morocco). It reveals two types of unusual magnetic fabrics. The first one is always located in the forelimb of the anticlines and is characterised by an oblique magnetic foliation with respect to bedding. The relationship between bedding and magnetic foliation indicates a sense of shear, which is consistent with the one expected from kinematic modelling. It is proposed that such an oblique magnetic foliation is the result of a weak strain that develops during folding. The other striking feature of the AMS results is that 40% of the magnetic lineations are parallel to the regional shortening direction. From structural and petrographical data, it is suggested that this magnetic lineation corresponds to the intersection lineation between two planar elements that are, respectively, the bedding and iron oxides mineralised veins. The latter result from iron-rich fluid circulations through a fracturing network.

Keywords: Hematite-bearing sandstones; Magnetic fabric; Fault-propagation fold; South Atlas Front, Morocco

1. Introduction

A fold-and-thrust belt is a transition zone between an apparently undeformed foreland and an internal domain characterised by high strain and metamorphism. In fold-and-thrust belts, sedimentary beds are folded and faulted but rocks do not show evidence of strong 'internal deformation' (strain). Nevertheless, several works (Averbuch et al., 1992, and references therein) have demonstrated that a weak internal deformation may occur and for this reason, some changes in the rock physical properties can be expected. Anisotropy of low field magnetic susceptibility (AMS) is a sensitive technique used in sedimentary rocks from fold-and-thrust belts for characterising and quantifying this cryptic deformation (e.g. Hrouda, 1991; Averbuch et al., 1992; Parés et al., 1999).

AMS provides information about the bulk preferred orientation of ferromagnetic/paramagnetic minerals and/or crystal lattices (Hrouda, 1982). It enables the definition of a magnetic fabric, which may be visualised as an ellipsoid whith principal axes $K1 \geqq K2 \geqq K3$. Basic elements of a magnetic fabric are the magnetic foliation (plane K1–K2) and the magnetic lineation (K1) when they are statistically defined. Both magnetic foliation and lineation are related to petrofabrics (e.g. Hrouda, 1982; Rochette et al., 1992; Borradaile and Henry, 1997).

The development of a thrust belt may generate two different types of strain:

1. Strain can be related to the development of a pre-folding layer parallel shortening (LPS) (Fig. 1a). LPS strain has been detected by means of magnetic fabric in limestones (Jackson et al., 1989; Aubourg et al., 1997), in sandstones and siltstones (Averbuch et al., 1992; Bakhtari et al., 1998) and in shales (Hirt et al., 1995; Parés et al., 1999). Although the amount of horizontal shortening is difficult to estimate, Hirt et al. (1995) or Sans et al. (1999) proposed that LPS can reach up to 20%. LPS-related

* Corresponding author. Tel.: +33-01-691567931; fax: +33-01-69154911.
E-mail addresses: stbezar@geol.u-psud.fr (B. Saint-Bezar).
[1] Present address: Département des Sciences de la Terre, UMR 8616, CNRS Orsayterre, Batiment 504, Universite de Paris-Sud, 91405 Orsay Cedex, France. Tel.: +33-(0)1-69-15-67-93; fax: +33-(0)1-69-15-49-11.

0191-8141/02/$ - see front matter
PII: S0191-8141(01)00140-7

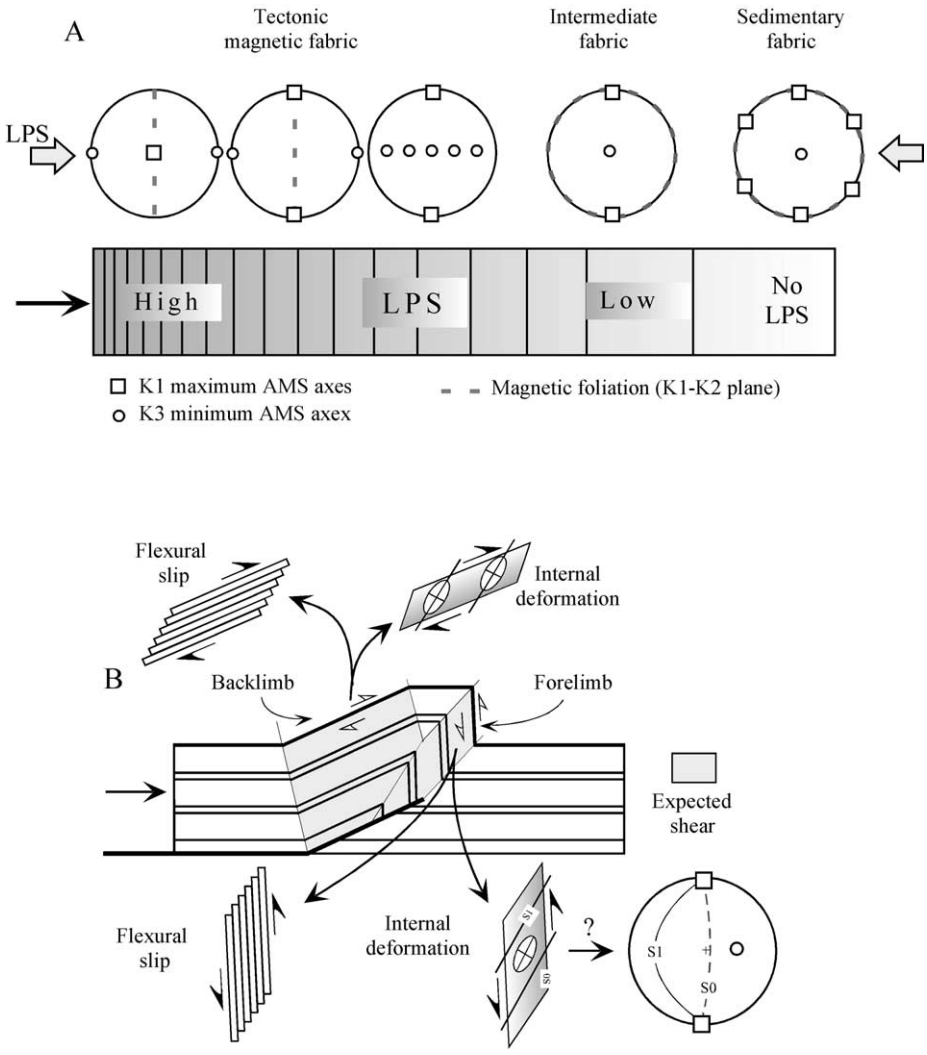

Fig. 1. (a) Sketch showing the evolution of the magnetic fabric in a LPS context (equal-area lower hemisphere projection). (b) Illustration of a fault-propagation fold with location of the expected shear zones. Deformation associated with folding may be accommodated by flexural slip or internal deformation. The resulting magnetic fabric due to internal deformation is also shown for the forelimb of the fold.

magnetic fabric results from coaxial deformation and shows the following typical evolution (Graham, 1966; Averbuch et al., 1992; Bakhtari et al., 1998) (Fig. 1a). It starts with a sedimentary magnetic fabric (i.e. no magnetic lineation and a magnetic foliation parallel to bedding) and ends with a tectonic magnetic fabric (i.e. magnetic foliation perpendicular to the bedding and the shortening direction). An intermediate magnetic fabric is defined by a magnetic lineation normal to the shortening direction and a magnetic foliation parallel to the bedding. This kind of intermediate magnetic fabric is common in thrust-and-fold belts (e.g. Bakhtari et al., 1998; Sagnotti et al., 1998; Parés et al., 1999, and references therein).

2. Strain can be related to folding (Fig. 1b). Kinematic models of ramp-related folding predict precisely the state of strain in the various parts of a given fold. This depends upon the folding modes: fault-bend folding (Suppe, 1983), fault-propagation folding (Suppe, 1985; Suppe and Medwedeff, 1990; Mercier et al., 1997) or trishear fault-propagation folding (Hardy and Ford, 1997; Allmendinger, 1998; Grelaud et al., 2000). Fig. 1b summarises the expected deformation within a single step fault-propagation fold. We focus on the forelimb because previous AMS studies, performed in regional scale fault-propagation folds (Averbuch et al., 1992; Frizon de Lamotte et al., 1997; Grelaud et al., 2000), have shown that strain is concentrated within the forelimb and close to the frontal hinges. Fig. 1b shows that deformation may be either accommodated by flexural slip and/or internal deformation such as bedding-parallel simple shear. In both cases the sense of shear is imposed by the chosen folding model.

This paper reports on a multidisciplinary investigation along a section across the South Atlas Front (Morocco). This frontal area exhibits a couple of fault propagation

folds previously described by Saint-Bezar et al. (1998). The present work aims to discuss the strain record of hematite-bearing sandstones that are involved within these folds.

2. Geological setting and sampling

The South Atlas Front corresponds to the southern deformation front of the Atlas Mountains (Frizon de Lamotte et al., 2000, and references therein). It represents the structural boundary between the Atlas Mountains and the Sahara platform belonging to the African Craton. The studied area is located along the Eastern High Atlas, north of the town of Goulmima (Fig. 2a).

South of Goulmima, the Anti-Atlas domain is made up of a Devonian carbonate platform, which overlies a Precambrian basement. Both units have been first deformed during the Variscan orogeny and then truncated by an erosional unconformity. Above the Devonian platform, the following sequence is observed: Upper Jurassic–Lower Cretaceous red sandstones and siltstones, Cenomanian–Turonian marine limestones and Senonian continental siltstones. This thin Mesozoic pile constitutes the Goulmima horizontal tableland, which bounds the Atlas Mountains.

North of the Goulmima tableland, the Mesozoic lithostratigraphic sequence is more complete (Bernasconi, 1983). It consists of red beds and basalts of Triassic age overlain by Lower to Middle Jurassic limestones. Upper Jurassic rocks are red continental sandstones/siltstones, which pass up into the Cretaceous sequence described above in the adjacent foreland.

From a structural point of view (Fig. 2), the region exhibits two major anticlines from south to north: the Tadighoust and the Jbel Ta'bbast anticlines. These folds have been developed at the tip of a southward propagating thrust fault following a general 'piggy-back' sequence. They have been modelled as fault propagation folds more or less altered by late evolution (Saint-Bezar et al., 1998). The two major structures are separated by a set of tight detachment folds accommodating a late transport on the upper flat of the Jbel Ta'bbast anticline (Fig. 2b). At outcrop scale, carbonate rocks involved in folds exhibit two major features: (i) normal-to-bedding stylolites, and (ii) parallel-to-bedding slickensides. Stylolites indicate a pre-folding LPS and slickensides can be related to syn-folding flexural slip. These elements are absent in the sandstones.

We sampled 34 sites (314 samples) along this cross-section (see Fig. 8a and b for location of the sites). Precise geographic locations are reported in Table 1. All the studied sites are in the Upper Jurassic–Lower Cretaceous red sandstones. They belong to the following structural positions: horizontal foreland (one site); forelimb of the Tadighoust anticline (eight sites); backlimb of the Tadighoust anticline (16 sites); intermediate area (five sites); forelimb of the Jbel Ta'bbast anticline (four sites).

3. Results

3.1. Petrography and magnetic mineralogy

The studied red sandstones are quartz-rich (Q: 75–85%) subarkoses or feldspathic subarkoses (F: 5–20%) that contain also minor amounts of rock fragments, very rare phyllosilicates and glauconite as well as heavy minerals, which are mainly opaque minerals. Quartz grains of these well to moderately-well sorted sandstones have in general a low sphericity and angular to sub-rounded morphology (Fig. 3a). It is consistent with their origin derived directly from the Panafrican or Variscan crystalline basement (Studer, 1980). The grain fabric shows the effects of pressure-solution processes during compaction with concavo–convex and sutured grain contacts (Fig. 3a–c). These subarkoses are cemented either by quartz overgrowth (Fig. 3c) or/and by a carbonate cement.

As demonstrated by reflected-light microscopy, SEM studies (Fig. 4) and microprobe analysis, the opaque minerals are primarily hematite and a small fraction is titanohematite. Two types of hematite grains are distinguished: (1) micron-sized detrital grains of hematite (Hem_D) concentrated along bedding-planes (Fig. 3d); (2) thin coatings of micron-sized crystals of hematite (Hem_C) around grains and within pores (Fig. 3e and f). This abundant and variable coating gives to the rock a pigmentation that is responsible for the red colour of the sediments. Regarding its spatial distribution, two possible origins for the thin hematite coatings may be considered. The first one assumes a detrital origin. In this case, it is older than compaction (Fig. 3e). The second one (Fig. 3f) is post compaction and might be diagenetic (Walker, 1967). For the latter, fine pigmentary hematite may be the result of a reprecipitation of iron deriving either from the alteration of Hem_D grains (Fig. 4) or from the in-situ destabilisation of phyllosilicate detrital grains. Neoformation of Hem_C from a hydrated iron oxide precursor such as goethite, which is in minor amount in some samples, can also be considered.

From the magnetic point of view, all the studied samples have a weak magnetic susceptibility, on average $K_m = 42 \pm 28$ μSI (Table 1). It is consistent with the low amount of ferromagnetic and paramagnetic grains observed in thin-sections. A stepwise demagnetisation of three orthogonal isothermal remanent magnetization (IRM; Lowrie, 1990) has been done on 10 samples. Hard, medium and soft coercivities range, respectively, in windows 0.5 T < hard < 1.1 T, 0.07 T < medium < 0.5 T and soft < 0.07 T. For each thermal step, the magnetic susceptibility has been measured in order to check if any magnetic mineralogy change occurred. A representative example of stepwise demagnetization of IRM is depicted in Fig. 5a. The medium and hard fractions of coercivities dominate with a maximum blocking temperature of 680 °C. This behaviour, which agrees with optical and SEM observations, suggests

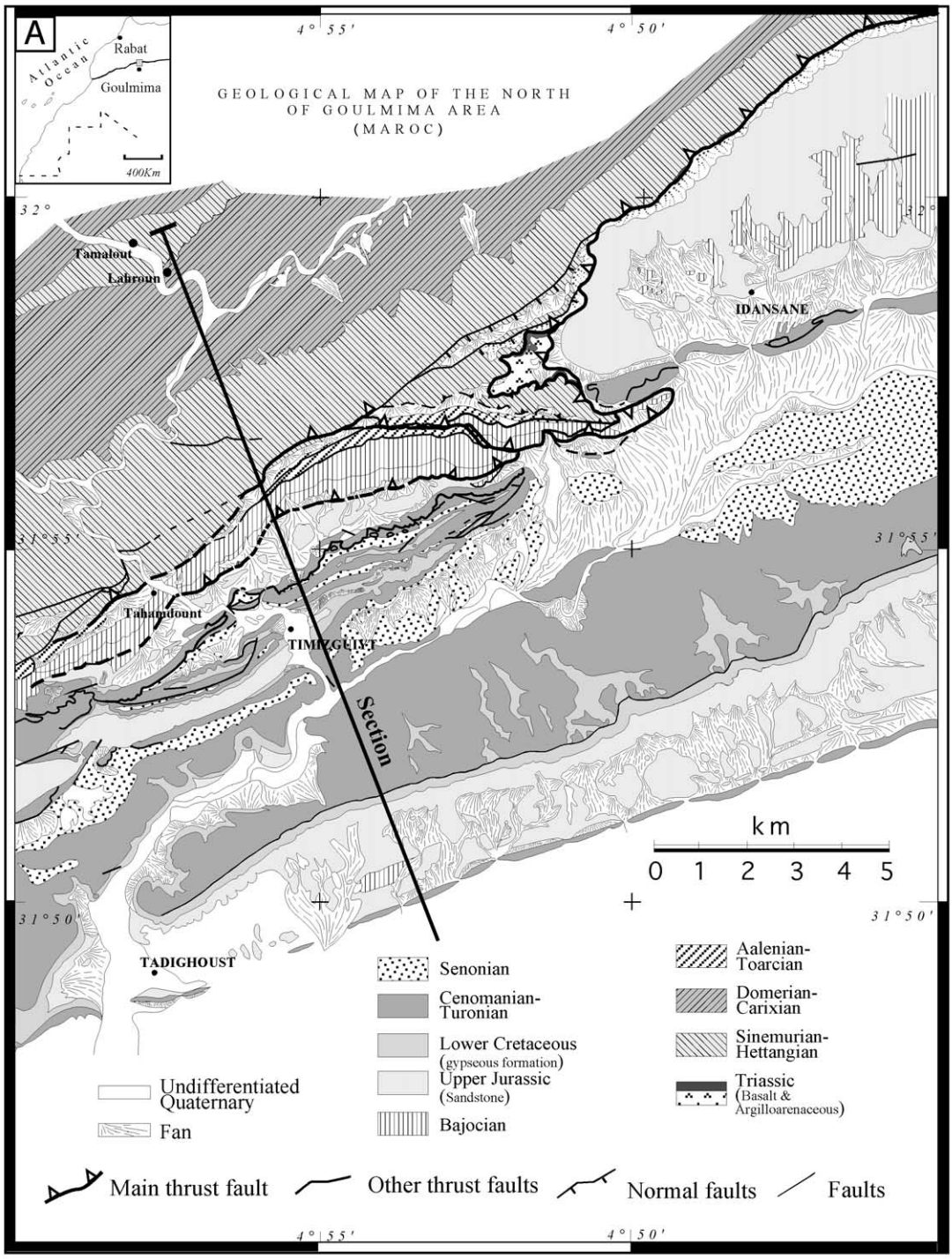
A
Atlantic Ocean
Rabat
Goulmima
400Km
GEOLOGICAL MAP OF THE NORTH OF GOULMIMA AREA (MAROC)
4° 55'
4° 50'
32°
31°55'
31°50'
Tamalout
Lahroun
IDANSANE
Tabamdount
TIMEZGUIWT
Section
TADIGHOUST
km
0 1 2 3 4 5
Undifferentiated Quaternary
Fan
Senonian
Cenomanian-Turonian
Lower Cretaceous (gypseous formation)
Upper Jurassic (Sandstone)
Bajocian
Aalenian-Toarcian
Domerian-Carixian
Sinemurian-Hettangian
Triassic (Basalt & Argilloarenaceous)
Main thrust fault
Other thrust faults
Normal faults
Faults

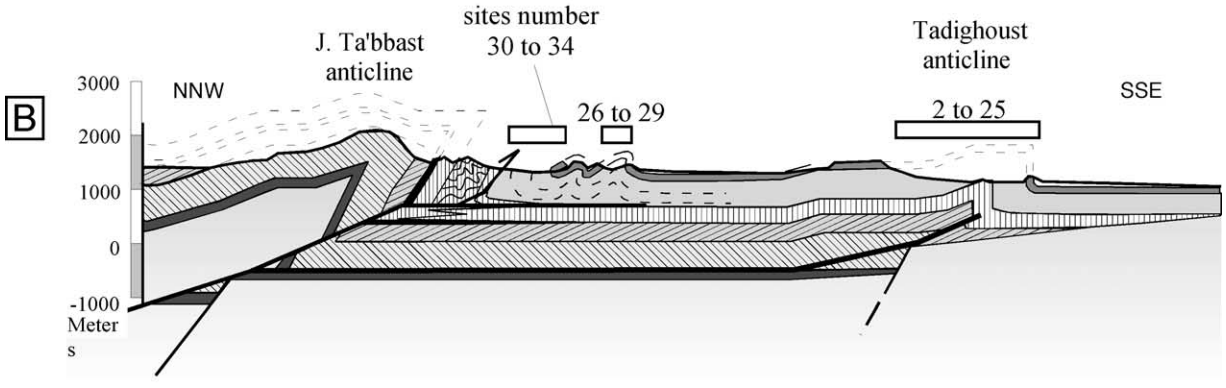
B
3000
2000
1000
0
-1000
Meters
NNW
J. Ta'bbast anticline
sites number 30 to 34
26 to 29
Tadighoust anticline
2 to 25
SSE

Table 1
AMS results. n: number of samples; $K_m = (K1 + K2 + K3)/3 K_m = (K1 + K2 + K3)/3$: mean susceptibility ($10^{-6}$ SI); $L = K1/K2$: lineation parameter; $F = K2/K3$: foliation parameter; $P_j = \exp\sqrt{2[(\eta1 - \eta_m)^2 + (\eta2 - \eta_m)^2 + (\eta3 - \eta_m)^2]}$: degree of anisotropy where $\eta1 = \ln K1$, $\eta2 = \ln K2$, $\eta3 = \ln K3$, $\eta m = (\eta1 + \eta2 + \eta3)/3$; $T_j = [2\ln(K2/K3)/\ln(K1/K3)] - 1$: shape parameter; K1g (D/I) and K3g (D/I): declination and inclination of K1 and K3 in geographic coordinates; K1t (D/I) and K3t (D/I): declination and inclination of K1 and K3 in tectonic coordinates; E (12/23/31): half confidence angles between K1 and K2, K2 and K3, K3 and K1; P.S0 (S/D): strike and dip of bedding (right hand rule); * for inverted beds

Text and captions site number	Sampled site number	Latitude	Longitude	n	K_m ($\times 10^{-6}$)	L	F	P_j	T_j	K1g (D/I)	K3g (D/I)	K1t (D/I)	K3t (D/I)	E (12/23/31)	P.S0 * (S/D)
1	96/11	31°42′15″	45°31′7″	9	150	1.010	1.032	1.044	0.517	253/1	140/86	253/1	140/86	24/6/6	Horizontal
2	96/5	31°50′14″	45°41′2″	5	11	1.024	1.055	1.083	0.385	99/13	214/61	56/36	310/21	38/22/15	245/70 *
3	95/1	31°50′09″	45°43′5″	9	32	1.009	1.120	1.146	0.855	247/6	6/79	70/11	172/48	47/5/4	85/53
4	00/19	31°50′03″	45°40′6″	9	45	1.004	1.006	1.001	0.175	34/60	176/25	189/13	316/69	27/25/16	255/80 *
5	00/21	31°50′01″	45°41′2″	8	86	1.002	1.034	1.041	0.882	70/11	161/5	66/2	180/85	30/7/11	250/85 *
6	00/18	31°50′06″	45°40′9″	9	49	1.011	1.015	1.026	0.151	258/5	164/8	251/1	345/69	15/15/7	75/80
7	00/23	31°50′06″	45°42′0″	8	22	1.005	1.016	1..022	0.492	77/34	342/8	108/13	316/80	19/10/6	76/65
8	00/16	31°50′07″	45°40′7″	9	45	1.003	1.021	1.026	0.719	73/44	336/7	117/12	307/78	35/11/8	70/75
9	96/4	31°50′15″	45°44′5″	8	32	1.023	1.005	1.030	− 0.630	117/60	307/29	136/9	242/61	11/79/11	69/57
10	00/13	31°50′27″	45°41′2″	11	33	1.003	1.025	1.030	0.781	344/4	110/84	194/15	346/75	37/7/5	240/20
11	00/12	31°50′31″	45°40′6″	10	21	1.003	1.022	1.028	0.791	271/1	179/70	91/10	271/80	46/4/11	242/24
12	95/2	31°50′25″	45°43′7″	13	23	1.011	1.084	1.105	0.756	328/9	119/80	148/6	344/84	19/3/8	226/20
13	96/3	31°50′40″	45°41′4″	7	56	1.003	1.004	1.007	0.027	233/0	139/85	233/2	354/86	11/16/5	249/9
14	00/11	31°50′33″	45°40′7″	11	38	1.006	1.020	1.028	0.532	237/2	142/70	244/15	13/67	20/11/7	255/35
15	00/10	31°50′35″	45°40′8″	10	38	1.003	1.011	1.014	0.606	288/7	170/74	107/12	300/70	46/12/5	235/27
16	00/9	31°50′36″	45°40′8″	10	29	1.003	1.018	1.023	0.678	349/7	187/82	173/13	333/76	28/10/9	255/15
17	00/8	31°50′37″	45°40′9″	9	36	1.005	1.009	1.013	0.303	70/2	220/87	70/4	322/76	21/8/5	242/15
18	00/7	31°50′40″	45°41′0″	13	30	1.005	1.019	1.025	0.554	291/10	156/74	113/4	341/83	33/8/12	260/18
19	00/6	31°50′43″	45°40′9″	10	33	1.005	1.018	1.025	0.535	68/9	186/71	67/6	210/82	26/3/10	260/13
20	00/5	31°50′43″	45°41′0″	6	131	1.001	1.003	1.005	0.530	337/18	179/70	338/7	192/82	40/12/25	260/12
21	00/4	31°50′47″	45°41′1″	13	42	1.005	1.032	1.040	0.721	146/0	238/85	145/12	335/77	22/6/8	265/10
22	96/2	31°50′50″	45°41′9″	10	50	1.010	1.037	1.051	0.558	268/1	172/75	89/13	270/77	39/5/12	220/20
23	96/1	31°49′30″	45°74′5″	7	42	1.010	1.034	1.046	0.558	262/12	138/69	168/14	58/74	22/7/4	270/25
24	00/1	31°51′01″	45°42′4″	9	26	1.011	1.017	1.028	0.182	4/32	185/59	1/17	202/72	4/12/6	255/15
25	00/2	31°50′58″	45°42′2″	9	26	1.013	1.008	1.021	− 0.210	306/1	209/85	226/6	308/84	20/37/13	259/9
26	95/3	31°53′10″	45°54′5″	9	37	1.030	1.088	1.125	0.483	43/5	294/75	54/13	155/38	25/24/3	55/65
27	96/6	31°53′22″	45°55′3″	8	43	1.012	1.026	1.039	0.342	47/18	310/19	63/4	193/84	18/12/15	45/76
28	95/8	31°54′15″	45°61′0″	9	27	1.005	1.041	1.051	0.784	190/10	351/86	7/0	109/88	35/14/6	Horizontal
29	95/4	31°53′22″	45°60′3″	6	12	1.013	1.034	1.049	0.445	221/0	131/34	232/13	76/76	55/24/7	239/53
30	95/5	31°54′22″	45°50′4″	8	35	1.004	1.066	1.079	0.893	243/5	90/84	243/7	23/6	58/15/11	243/17
31	96/8	31°54′35″	45°62′2″	12	46	1.019	1.008	1.028	− 0.429	49/9	157/63	229/8	351/75	10/17/9	247/44 *
32	96/10	31°54′32″	45°61′5″	9	32	1.015	1.011	1.026	− 0.154	23/2	120/72	207/9	324/71	27/46/5	218/40 *
33	95/6	31°54′29″	45°64′0″	16	26	1.014	1.056	1.075	0.586	228/5	341/78	233/10	333/46	29/11/6	240/32 *
34	96/9	31°54′20″	45°70′7″	7	41	1.004	1.005	1.011	0.063	45/16	212/74	36/2	304/44	40/25/24	235/51 *

Fig. 2. (a) Geological map of the South Atlas Front in the studied area (from Saint-Bezar, 1999). (b) Modelled cross-section (Saint-Bezar et al., 1998) with same geological patterns as in (a).

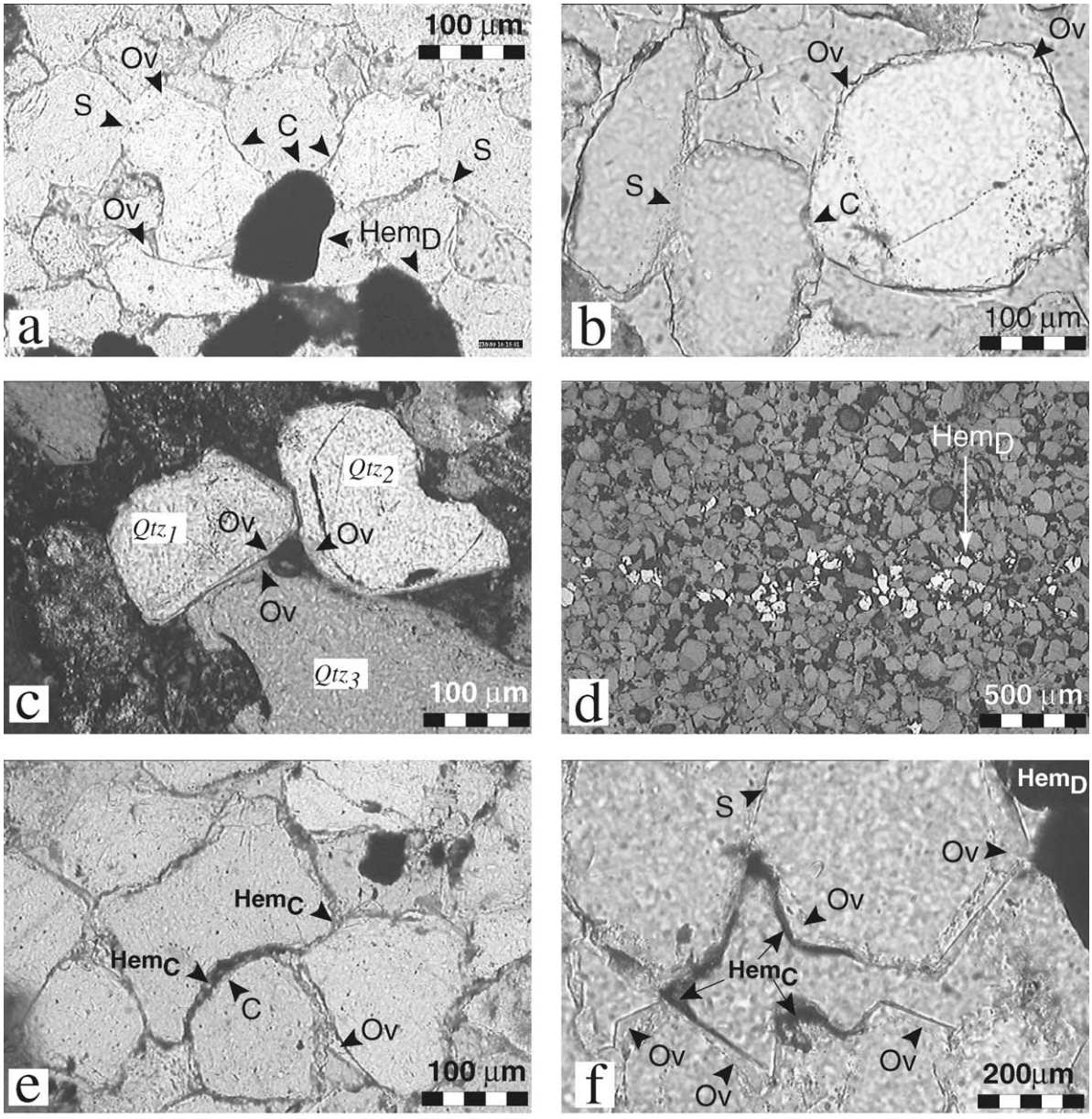

Fig. 3. (a) Plane polarized light (PPL) microphotograph of a carbonate cemented subarkose (site 31). Quartz grains, with some exceptions, have an overall low sphericity. They display a broad range of shape parameters from angular to sub-rounded morphology. Note the nature of the contacts between grains (S: sutured grains; C: concavo–convex contacts) as well as the presence of very thin quartz overgrowths (Ov) around some detrital quartz grains. Note also the detrital hematite grains (Hem_D) in the lower part of the microphotograph. They show concavo–convex contacts with neighbouring quartz grains. (b) Detail on grain relationships within subarkose (site 16; PPL microphotograph). Sutured quartz grains (S) and concavo–convex contacts (C) result from pressure-solution during compaction. Note that the shape of the detrital grains is still observable and that tiny quartz overgrowths (Ov) wrap some of the detrital grains. (c) PPL microphotograph of quartz cemented subarkose (site 3). Quartz overgrowths (Ov) around three quartz grains (respectively, Qtz1, Qtz2 and Qtz3) cause an important porosity loss. The three overgrowth phases form a triple junction within the pore. Unfortunately this triple junction is partially hidden by a trapped air bubble within the resin of the thin-section. (d) Concentration of opaque minerals (white to light grey) along bedding planes (site 23; reflected light microphotograph). (e) Distribution of hematite coating (Hem_C) within subarkose (PPL microphotograph, site 32). The occurrence of Hem_C trapped within a concavo–convex contact between quartz grains suggests a pre-compaction origin. (f) Hematite coating (Hem_C) distribution: (i) sutured contacts between quartz grains are free of Hem_C, and (ii) Hem_C is located along pore walls and clearly postdates quartz-overgrowths. This texture supports a post-compaction origin for Hem_C. (site 23; PPL microphotograph).

that coarse hematite is the main magnetic carrier mineral. The thermal evolution of the soft coercivity displays a lower unblocking temperature (between 550 and 680 °C). This could be caused by two populations of carrier minerals. Polished thin section analyses do not reveal any occurrence of magnetite. The absence of magnetite is supported by IRM acquisition (Fig. 5b) where saturation is only approached at the end of the experiment for a 1200 mT applied field. Consequently, the soft coercivity fraction is probably due to small amounts of titanohematites.

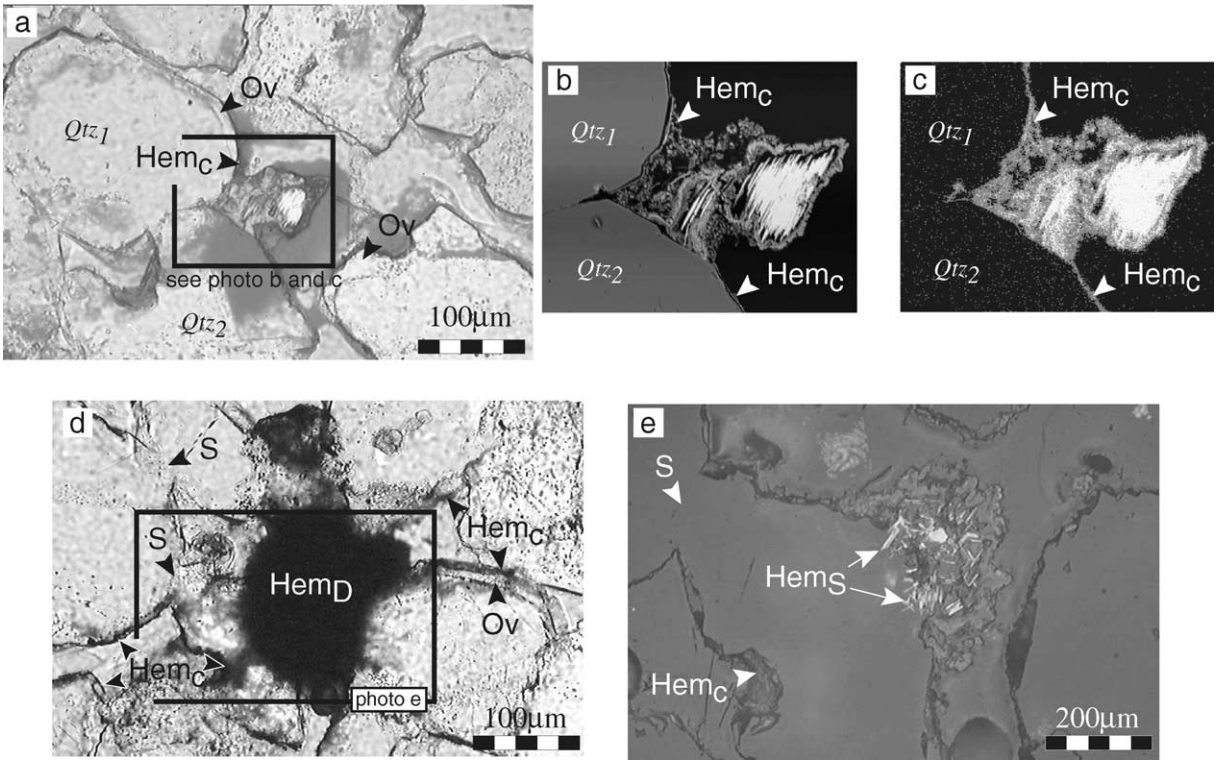

Fig. 4. (a) Example of detrital origin of hematite between quartz detritals with overgrowth phases (in mixed PPL and reflected light). (b) Enlarged back-scattered electron image of hematite from (a). (c) Iron mapping image (SEM) of (b) showing that iron oxide occurs as: (i) a corona around the hematite detrital grain, and (ii) a coating. It suggests a mobility of iron resulting from the hematite grain alteration. Note that Hem_C is wrapping quartz overgrowths (see (a)) and that there is no iron-bearing oxide at the contact between the two adjacent quartz grains. This suggests a post-diagenetic and post-compaction origin for Hem_C. (d) PPL microphotograph of a detrital grain of hematite (Hem_D). (e) Enlarged reflected light microphotograph of Hem_D grain from (d). It shows the new growth of very fine acicular crystals of hematite (Hem_S).

3.2. Magnetic fabric results

The anisotropy of low-field magnetic susceptibility (AMS) was measured using Agico kappabridges KLY-2 and KLY-3, following the procedures of Jelinek (1977). The mean tensorial statistics method of Jelinek (1978) was applied. AMS results are compiled in Table 1. Samples with poorly defined directions, i.e. with confidence angles greater than 30°, have been rejected. This sorting does not affect the calculation of the mean tensorial AMS axes (Jelinek, 1978).

The shape of the AMS ellipsoid may be shown in a P_j vs. T_j diagram (Jelinek, 1981) (Fig. 6). T_j reflects the shape of the AMS ellipsoid and P' the degree of anisotropy. The shape of the magnetic fabric is essentially oblate (the average for all the sites is $T_j = 0.42 \pm 0.37$). Only four sites (9, 25, 31 and 32; Table 1) have a prolate fabric. P_j ranges from low values of 1.007 up to 1.125. The mean value of P_j ($P_j = 1.041 \pm 0.032$) is typical of weakly deformed rocks (Hrouda, 1982). Relatively high values of $P_j > 1.05$ are compatible with the high intrinsic planar anisotropy of hematite (K1/K3 ~ 100) (Rochette et al., 1992). Note that there is no controlled spatial distribution of anisotropy parameters within the fold.

Magnetic fabrics are generally well-defined. In the following section, we will present firstly the geometry of the magnetic foliation and secondly, the magnetic lineation directions. For this purpose, we have selected four sites which are considered representative of the overall measured magnetic fabrics. For each representative site, the data are plotted after bedding correction (Fig. 7).

About 80% of the sites show a magnetic foliation, which is statistically parallel to bedding (Fig. 7a). In these cases, the ellipse of confidence of the tensorial mean K3 includes the pole of the bedding or is close to it. About 5% of the sites exhibit a zonal dispersion of the magnetic foliations (K3 axes) parallel to the shortening direction (Fig. 7b). The last 15% of the sites show a mean magnetic foliation statistically oblique to the bedding (Fig. 7c). In this case, the tensorial mean of the magnetic foliation poles (K3) is clearly different from the pole of bedding.

The direction of the magnetic lineations is more difficult to appreciate. We consider that there is no magnetic lineation when: (i) K1 is visually scattered, and (ii) the confidence angle of tensorial mean of the magnetic lineations is large (E12 > 35°; Table 1). According to these criteria, 25% of the sites have no magnetic lineation (Fig. 7a). In about 45% of the sites, the magnetic lineation is more or less parallel to the fold axis (i.e. within the SW–NE quadrant; Fig. 7b and c). Eventually, the last 30% of the

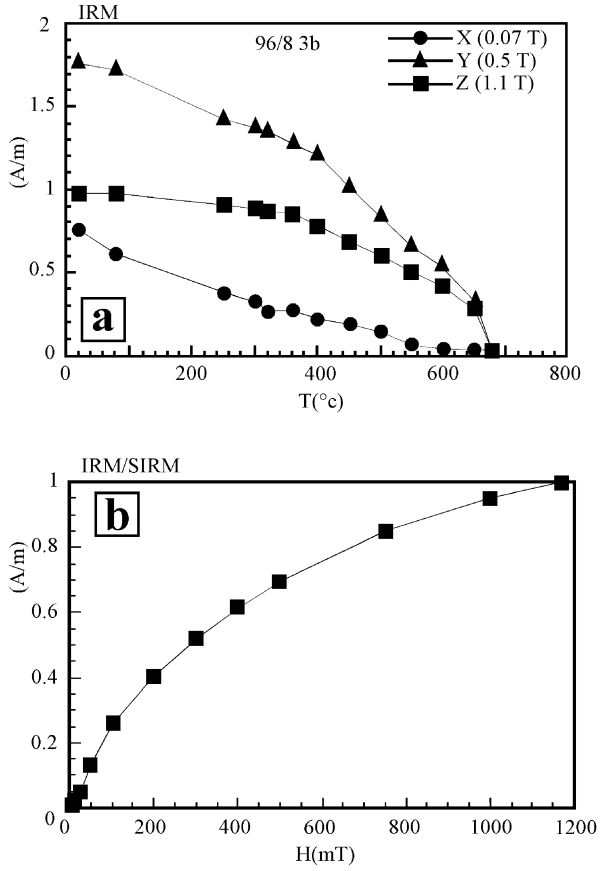

Fig. 5. (a) Representative example of demagnetisation curves (site 31). See explanation in text. (b) IRM acquisition curve up to 1200 mT normalised to the saturation IRM at room temperature.

sites are characterised by magnetic lineations that are roughly perpendicular to the fold axis (i.e. within the NW–SE quadrant; Fig. 7d).

All the magnetic fabric data (in in-situ coordinates) are reported along the cross-section (Fig. 8a and b).

Along the Tadighoust anticline (Fig. 8a), 16 sites are located within the backlimb, while eight sites are close to the hinge or in the forelimb. In the backlimb, the magnetic foliation is always parallel to bedding, whilst in the forelimb

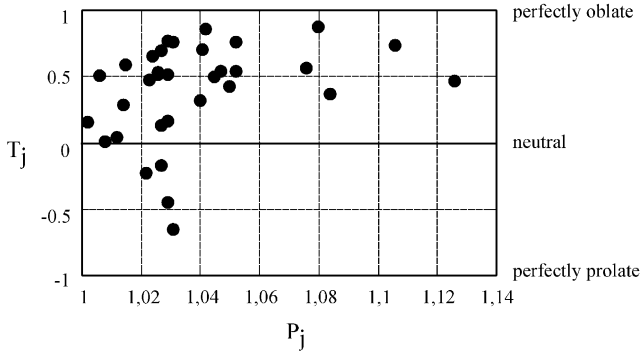

Fig. 6. Degree of anisotropy (P_j) vs. shape parameter T_j. See definitions of these two parameters in Table 1.

it is either parallel (75%) or oblique (25%) to bedding. The magnetic lineations in both parts of the anticline are roughly fold-parallel (i.e. in the NE–SW quadrant) or fold-perpendicular (i.e. in the NW–SE quadrant).

Between the Tadighoust (Fig. 8a) and Jbel Ta'bbast anticlines (Fig. 8b), five sites are located in the minor disharmonic detachment folds. The magnetic foliations are parallel to bedding except for site 26. Though the magnetic lineations are poorly defined, their means are roughly parallel to the fold axis. Four sites are located in the overturned forelimb of the Jbel Ta'bbast anticline (Fig. 8b). They show either magnetic foliations that are oblique to bedding (sites 33 and 34) or a girdled distribution (sites 31 and 32) around the magnetic lineation. Note that sites 31 and 32 have: (i) negative T_j values (see Table 1), which indicates a prolate shape, and (ii) a girdle distribution of K3 axes (Fig. 8b). These two features suggest the superposition of two flattenings. In conclusion, from sites 31 to 34, we observe the progressive disappearance of a sedimentary imprint and its replacement by a new magnetic foliation, which is different from the bedding. Note also that the magnetic lineation is parallel to the fold axis for these four sites.

Because of poor exposure of the unfolded foreland, only one site has been sampled in this domain (Site 1, Fig. 8a). It is located about 14 km south of the Tadighoust anticline. This site is characterised by a foliation parallel to bedding and a poorly defined magnetic lineation (E–W on average).

One of the most striking features of these results is that oblique magnetic foliations are always located within the forelimb of the anticlines. Another one is that magnetic lineations are either parallel or perpendicular to the fold axis. These two different points will be discussed in the following section.

4. Discussion

Previous studies (Graham, 1966; Kissel et al., 1986; Jackson et al., 1989; Lee et al., 1990; Averbuch et al., 1992; Frizon de Lamotte et al., 1997; Parés et al., 1999) provide good examples of the kind of magnetic fabric evolution in a fold-and-thrust belt that is nowadays widely accepted (Fig. 1a). The magnetic foliation evolves through the belt. It is parallel to the bedding in the foreland domain (sedimentary magnetic fabric); it is vertical to the bedding and normal to the shortening direction (tectonic magnetic fabric) in the most deformed domain (i.e. the front of the belt); in between these two magnetic foliation end-members, an intermediate fabric, characterised by the loss of magnetic foliation (girdle distribution of K3 axes in the shortening direction), results from the competition between a primary sedimentary magnetic fabric and an overprinting tectonic magnetic fabric (Fig. 1a). Note that the magnetic lineation, when it appears, is always normal to the shortening direction. All the previously mentioned studies argue for

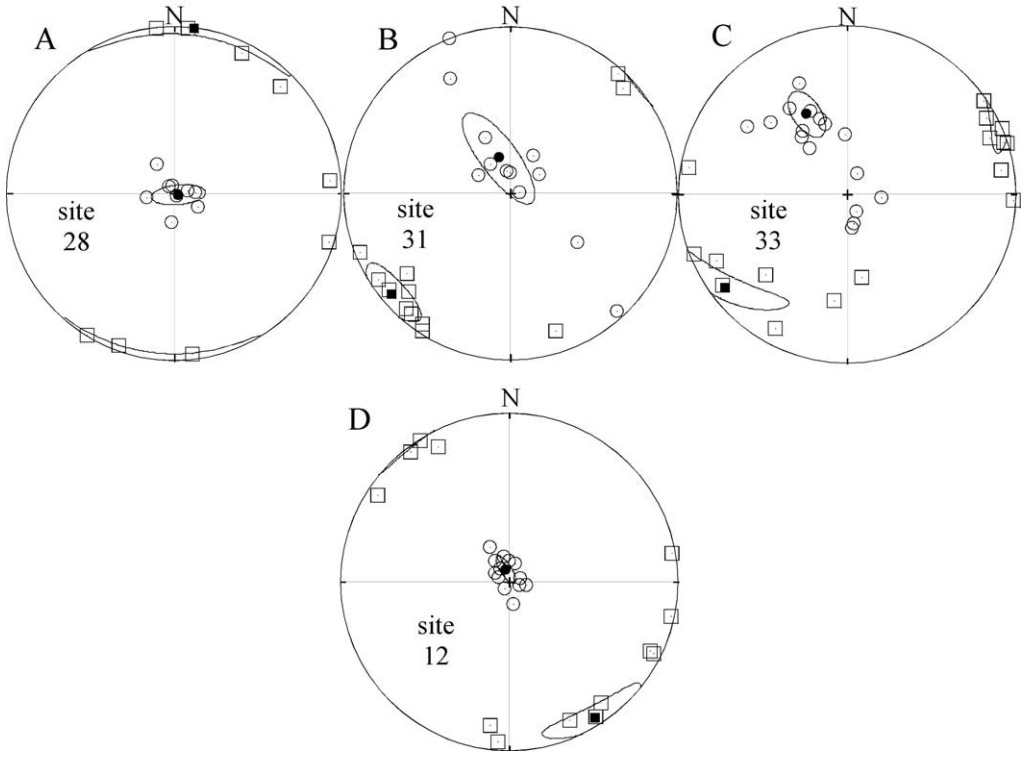

Fig. 7. Representative examples of AMS magnetic fabrics after bedding correction. K1 (white square), K1 mean tensorial (black square), K3 (white circle) and K3 mean tensorial (black circle).

an early development of an LPS-related magnetic foliation that was acquired when the bedding was still horizontal.

The results of this AMS study show four types of magnetic fabric: (i) a sedimentary fabric localised in the undeformed foreland, (ii) intermediate fabrics, (iii) tectonic fabrics with a girdle distribution of K3 axes parallel to the shortening direction, and (iv) unusual tectonic fabrics characterised by a magnetic foliation that is oblique to the bedding. Note that in this study, we never observe the ultimate stage of tectonic magnetic fabric characterised by a magnetic foliation perpendicular to the bedding (see Figs. 1a and 8a and b). The three first types are consistent with the magnetic fabric evolution related to the LPS development. The fourth type, by contrast, cannot be interpreted in a LPS context and implies a different mechanism of deformation.

Let us focus on this unusual magnetic fabric. According to fault propagation fold kinematic modelling (Suppe, 1983, 1985; Suppe and Medwedeff, 1990; Mercier et al., 1997), folds grow by hinge migration. Deformation within the limbs is acquired when rock passes through the hinges. From a finite strain point of view, it behaves as if the limbs of the folds rotate instantaneously and that bedding parallel simple shear (Fig. 1b) accommodates the deformation. The more important the rotation of the limb, the more important the rate of simple shear. Consequently, in the case of an asymmetrical fault propagation fold, such as the Jbel Ta'bbast and the Tadighoust anticlines (Saint-Bezar et al., 1998), the deformation must be more important in the forelimb than in the backlimb. In this study, oblique magnetic foliations represent the most evolved magnetic fabrics that have been measured. Firstly, they are always located within the forelimb of the anticlines, which agrees with the above consideration. Secondly, considering that magnetic foliation can be regarded as a cryptic cleavage (e.g. Hrouda, 1982), its geometrical relationship with the bedding enables the deduction of a sense of shear that is consistent with the one expected in the forelimb of a fault-propagation fold (Fig. 1b). Therefore, the formation of such an oblique magnetic foliation in this part of the fold suggests that deformation related to fold growth is also accommodated by internal deformation. In this case, the magnetic fabric is the result of a syn-folding record.

The other striking feature of our magnetic fabrics is that about 30% of the magnetic lineations are perpendicular to the fold axes (i.e. parallel to the shortening direction). It is a very puzzling feature because magnetic lineations are almost always parallel to the fold axes in fold-and-thrust belts (e.g. Lee et al., 1990; Hrouda, 1991; Sagnotti et al., 1998; Grelaud et al., 2000). Before interpreting these unusual fabrics, it is important to note that hematite is the magnetic carrier of the studied sandstones and that it is also an original feature of this work. Hematite has a triaxial and a strong oblate magnetocrystalline anisotropy (Rochette et al., 1992). For this reason, a magnetic lineation in hematite-bearing sandstones can be explained as the result of a crenulation of platy hematite along a zonal axis (Lamarche and

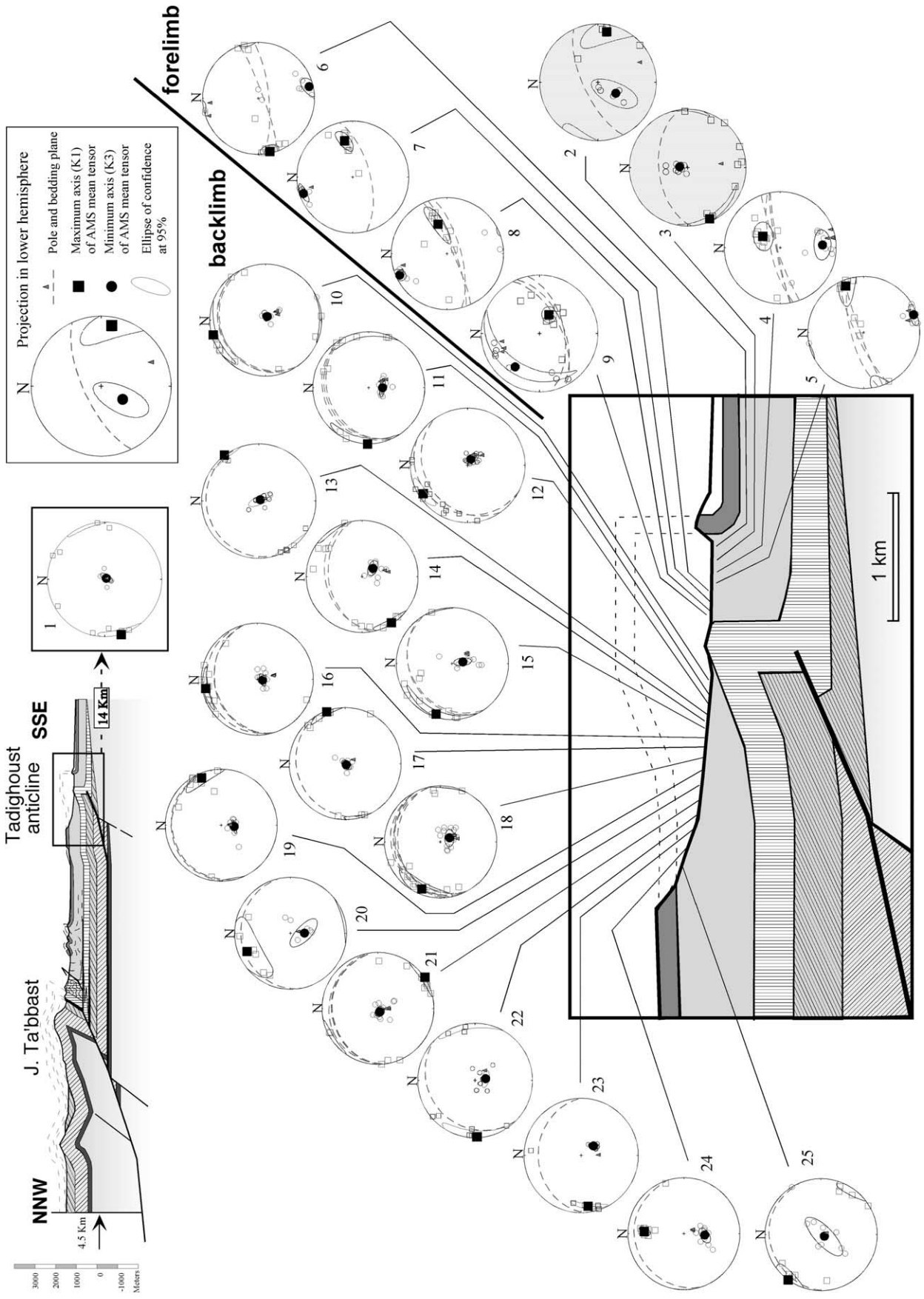

Fig. 8. Representation of AMS results (in geographic coordinates) according to sampling sites. (a) Along the southern part of the cross-section. (b) Along the northern part of the cross-section. Grey-shaded stereograms are for oblique magnetic foliations.

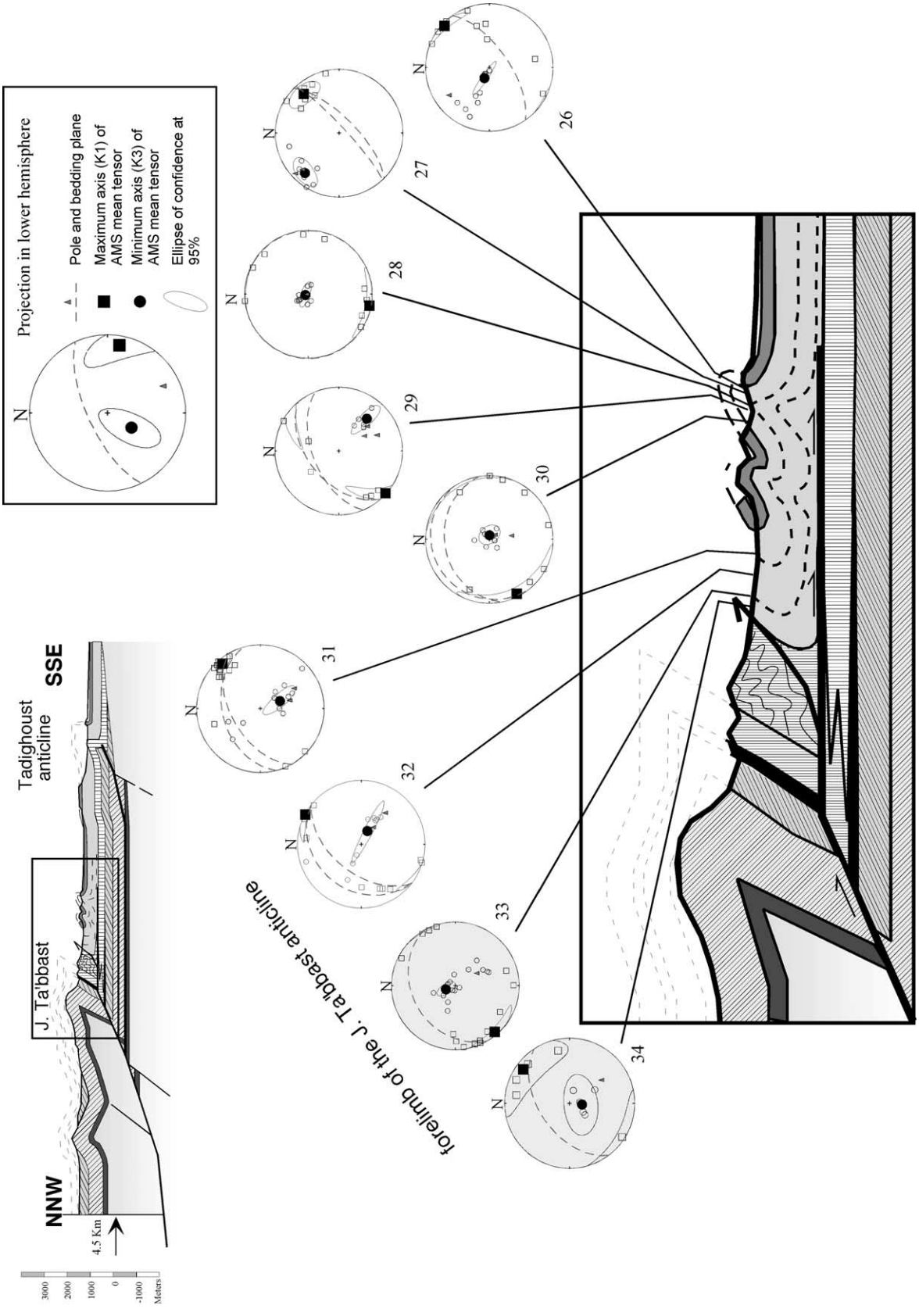

Fig. 8. (*continued*)

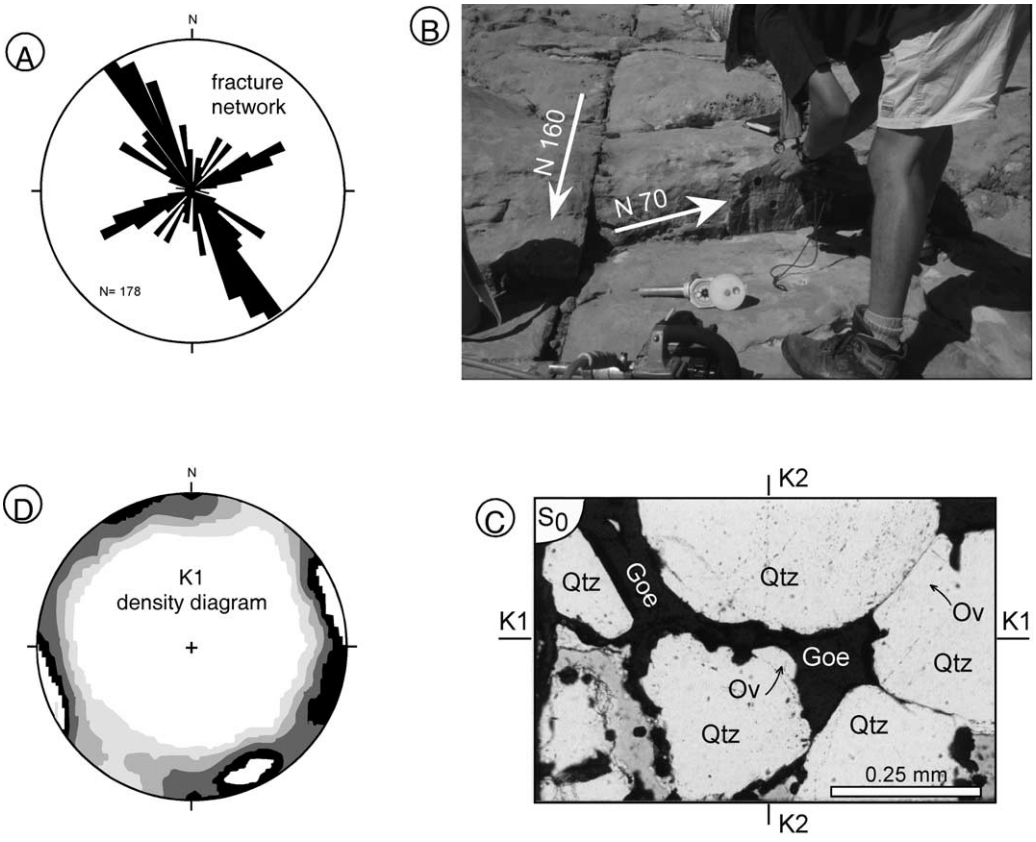

Fig. 9. (a) Rose diagram of the Tadighoust anticline fracturing network. There are two main orthogonal directions, N 150–160° is dominant. (b) Field example (site 20) of the two main fracturing directions. Iron rich precipitation testifies for preferential fluid flow circulation along these fractures. (c) Oriented thin section (site 20) with K1 parallel to the shortening direction. Coarse goethite fills oversized pores and quartz grains show etching pits. This suggests a precipitation of goethite from iron-rich fluids that have been channelled along preferred directions. (d) Contoured diagram of all the K1 axes measured on the Tadighoust anticline (after bedding correction). Note the correspondence between the two principal directions of K1 axes and the main fracture directions of (a).

Rochette, 1987). In that case, the resulting magnetic lineation is trending normal to the shortening direction. This interpretation gives an explanation for all the fold parallel magnetic lineations but not for the 30% of fold perpendicular magnetic lineations of this study. Indeed, it would imply an ENE–WSW compressive event for which there is no evidence throughout the Atlas belt.

So what are the other possible explanations for the shortening-parallel magnetic lineations?

1. The acquisition of a syn-sedimentary magnetic lineation due to depositional paleocurrents is unrealistic because it would imply a constant direction of currents over 70 Ma (the studied red sandstones span from the Upper Jurassic up to the Lower Cretaceous). In addition, there is no magnetic lineation in the unfolded foreland (site 1, Fig. 8a; dispersion of K1 axes within the bedding plane). Therefore, the magnetic lineations in the deformed area that are either fold-parallel or fold-perpendicular are likely to be of tectonic origin.
2. Hematite is not subject to interchange of AMS axes (for a comprehensive review see Rochette et al., 1992) as may be the case in fine magnetite grains. In order to test inverse fabric, we measured AIRM (anisotropy of isothermal remanent magnetisation) of representative sites (not shown) and found similar AMS and AIRM. For this reason, the hypothesis of inverse magnetic fabrics can also be rejected.
3. "Transport parallel magnetic lineations" have already been described by Aubourg et al. (1991, 1999) in the subalpine chains. These lineations, which have been measured in strained black shales within a décollement level, are interpreted as the result of stretching parallel to tectonic transport. Such an interpretation is unlikely because sandstones from our study pertain to a quite different tectonic context (folded cover vs. décollement level).
4. According to Borradaile and Tarling (1981), the magnetic lineation in deformed sedimentary rocks may be the result of a competition between two magnetic fabrics. It is a common interpretation for fold-parallel magnetic lineations (see above references) where it corresponds to the intersection in between a sedimentary magnetic fabric (the bedding) and a vertical magnetic

fabric (e.g. stylolitic joints related to LPS). The result of numerical modelling (Housen et al., 1993) shows also that the combination of two magnetic foliations produces a magnetic lineation at the intersection of the two planar elements.

Taking into account this latter concept, we can now propose an alternative explanation constrained by field observations, petrographic data and AMS results.

Field observations show: (i) a joint system made of two orthogonal systematic fracture sets. The predominant joint set is orientated roughly NNW–SSE, whilst the second one trends ENE–WSW (Fig. 9a). The development of this network is consistent with the regional shortening direction; (ii) a network of massive and diffuse veins (Fig. 9b). These veins suggest fluid flow along structural directions similar to the fracture network.

The study of orientated thin sections reveals: (i) fine pigmentary hematite of detrital origin (Hem_C; Fig. 3e and f); (ii) a pervasive precipitation of goethite within massive veins with fuzzy boundaries (Fig. 9b and c) derived from iron-rich fluids that have been channelled along preferred directions. This coarse goethite (Fig. 9c), is filling oversized pores resulting from the partial or total dissolution of quartz grains. It suggests a circulation of iron rich fluids post-dating sedimentary and tectonic (LPS) compactions.

Eventually, the contoured stereogram of K1 axes (Fig. 9d) shows that magnetic lineations are distributed around two directions, which are coaxial with the fracturing directions. A consistent relationship between the structural and the AMS data can thus be established.

Taking into account all these data, it is proposed that magnetic lineations parallel to the shortening direction are the result of the intersection between two planar elements, i.e. the bedding and a new magnetic foliation materialised by goethite-mineralised veins.

5. Conclusions

The AMS investigation within the folded foreland of the High Atlas shows the following results:

1. An evolution of the magnetic fabric from an undeformed foreland (sedimentary magnetic fabric) to a deformed domain (tectonic magnetic fabrics). Between these two end-members, 75% of the magnetic fabrics are of intermediate type.
2. 60% of the magnetic lineations are fold-parallel, i.e. normal to the shortening direction.

These two results are similar to that classically reported in fold-and-thrust belts.

1. Amongst the tectonic magnetic fabrics, when a magnetic foliation is well defined, it appears to be always oblique to bedding and always located in the forelimb of the folds where the deformation is expected to be the strongest (Fig. 1). In addition, the geometrical relationship between the magnetic foliation and the bedding provides a sense of shear that is consistent with that predicted by kinematic models.
2. 40% of the magnetic lineations are fold perpendicular, i.e. parallel to the shortening direction.

These two results are unusual and new compared with other AMS studies performed in fold-and-thrust belts. The presence of oblique magnetic foliations suggests that, in addition to flexural slip, the deformation during the growth of a fault-propagation fold may also be accommodated by strain and that this strain seems to develop primarily in the forelimb.

Concerning the occurrence of magnetic lineation parallel to the regional shortening direction, it is proposed that it could result from the intersection of two magnetic foliations, i.e. a magnetic sedimentary foliation (parallel to bedding) and a new vertical magnetic foliation. This second planar element is thought to correspond to the observed iron-rich mineralised veins (the measured magnetic lineation cannot be of textural origin because sampling is not restricted to the veins). The latter result from fluid flow through preferred pathways that have coeval directions with the regional deformation pattern. These fluid circulations clearly post-date vertical (sedimentary) and horizontal (LPS) compactions, and they likely occurred during folding.

This study suggests that the interpretation of magnetic lineation in terms of intersection lineation of a flattening plane (such as usual LPS joints) and bedding is not always straightforward. Therefore, the geological significance of AMS data must always be constrained with structural and petrographical observations.

Acknowledgements

This work, which is a part of a PhD, has been carried out by B. Saint-Bezar at the University of Cergy–Pontoise (France) and completed at the Katholieke Universiteit of Leuven (Belgium) under a post-doctoral fellowship. BSB, RH and CA would like to acknowledge the Ministère de l'Energie et des Mines de Rabat (Maroc) and the Local authorities of Goulmima for their assistance. We would like to acknowledge Dr A. Hirt and Dr B. Housen for their reviews, as well as Matteo Molinaro for his reading. Special thanks to Odile Blanchet for her logistic help.

References

Allmendinger, R.W., 1998. Inversed forward numerical modelling of trishear fault propagation fold. Tectonics 17, 640–656.

Aubourg, C., Rochette, P., Vialon, P., 1991. Subtle stretching lineation revealed by magnetic fabric of Callovian–Oxfordian black shales (French Alps). Tectonophysics 185, 211–223.

Aubourg, C., Frizon de Lamotte, D., Poisson, A., Mercier, E., 1997. Magnetic fabrics and oblique ramp-related folding. A case study from the Western Taurus (Turkey). J. Struct. Geol. 19, 1111–1120.

Aubourg, C., Rochette, P., Stéphan, J.F., Popoff, M., Chabert-Pelline, C., 1999. The magnetic fabric of weakly deformed late Jurassic shales from the Southern Subalpine Chains (French Alps). Evidence for SW-directed transport direction. Tectonophysics 307, 15–32.

Averbuch, O., Frizon de Lamotte, D., Kissel, C., 1992. Magnetic fabric as a structural indicator of the deformation path within a fold thrust structure: a test case from the Corbières (NE Pyrenees, France). J. Struct. Geol. 14, 461–474.

Bakhtari, H., Frizon de Lamotte, D., Aubourg, C., Hassanzadeh, J., 1998. Magnetic fabric of Tertiary sandstones from the Arc of Fars (Eastern Zagros, Iran). Tectonophysics 284, 299–316.

Bernasconi, R., 1983. Géologie du Haut Atlas de Rich (Maroc). Thèse es Sciences, Université de Neuchâtel, 107pp.

Borradaile, G., Tarling, D.H., 1981. The influence of deformation mechanisms on magnetic fabrics in weakly deformed rocks. Tectonophysics 77, 151–168.

Borradaile, G.J., Henry, B., 1997. Tectonic applications of magnetic susceptibility and its anisotropy. Earth Sci. Rev. 42, 49–93.

Frizon de Lamotte, D., Mercier, E., Dupré La Tour, A., Robion, P., Averbuch, O., 1997. Cinématique du Plissement et Déformation Interne des Roches: l'exemple du pli de Lagrasse (Aude, France). C. r. Acad. Sci. Paris 324, 591–598.

Frizon de Lamotte, D., Saint-Bezar, B., Bracène, R., Mercier, E., 2000. The two main steps of the Atlas building and geodynamics of the western Mediterranean. Tectonics 19, 740–761.

Graham, J.W., 1966. Significance of magnetic anisotropy in Appalachian sedimentary rocks. In: Steinhart, J.S., Smith, T.J. (Eds.). The Earth Beneath the Continents. Am. Geophys. Union, Washington, pp. 627–648 Geophysical Monograph 10.

Grelaud, S., Buil, D., Hardy, S., Frizon de Lamotte, D., 2000. Trishear kinematic model of fault-propagation folding and sequential development of minor structures: the Oupia anticline (NE Pyrenees, France). Bull. Soc. géol. Fr. 171, 441–449.

Hardy, S., Ford, M., 1997. Numerical modeling of trishear fault propagation folding and associated growth strata. Tectonics 16, 841–854.

Hirt, A.M., Evans, K.F., Engalder, T., 1995. Correlation between magnetic anisotropy and fabric for Devonian shales on the Appalachian plateau. Tectonophysics 247, 121–132.

Housen, B.A., Richter, C., Van der Pluijm, B.A., 1993. Composite magnetic anisotropy fabrics: experiments, numerical models, and implications for the quantification of rocks fabrics. Tectonophysics 200, 1–12.

Hrouda, F., 1982. Magnetic anisotropy of rocks and its application in geology and geophysics. Geophys. Surveys 5, 37–82.

Hrouda, F., 1991. Models of magnetic anisotropy variations in sedimentary thrust sheets. Tectonophysics 185, 203–210.

Jackson, M., Craddock, J.P., Ballard, M., Van der Voo, R., McCabe, C., 1989. Anhysteretic remanent magnetic anisotropy and calcite strains in Devonian carbonates from the Appalachian Plateau, New York. Tectonophysics 161, 43–53.

Jelinek, V., 1977. The statistical theory of measuring anisotropy of magnetic susceptibility on groups of specimens and its application. Geofyzyca, 1–88.

Jelinek, V., 1978. Statistical processing of anisotropy of magnetic susceptibility measured on groups of specimens. Studia Geoph. et Geod. 22, 50–62.

Jelinek, V., 1981. Characterization of the magnetic fabric of the rocks. Tectonophysics 79, 63–67.

Kissel, C., Barrier, E., Laj, C., Lei, T.Q., 1986. Magnetic fabric in "undeformed" marine clays from compressional zones. Tectonics 5, 769–781.

Lamarche, G., Rochette, P., 1987. Microstructural analysis and origin of lineations in the magnetic fabric of some Alpine slates. Tectonophysics 139, 285–293.

Lee, T.-Q., Kissel, C., Laj, C., Chorn-Shern, H., Yi-Teh, L., 1990. Magnetic fabric analysis of the Plio-Pleistocene sedimentary formations of the coastal range of Taiwan. Earth Planet Sci. Lett. 98, 23–32.

Lowrie, W., 1990. Identification of ferromagnetic minerals in rock by coercitivity and unblocking temperature properties. Geophys. Res. Lett. 17, 159–162.

Mercier, E., Outtani, F., Frizon de Lamotte, D., 1997. Late evolution of fault-propagation folds: principles and example. J. Struct. Geol. 19, 185–193.

Parés, J.P., van der Pluijm, B.A., Dinarès-Turell, J., 1999. Evolution of magnetic fabric during incipient deformation of mudrocks (Pyrenees, Northern Spain). Tectonophysics 307, 1–14.

Rochette, P., Jackson, J., Aubourg, C., 1992. Rock magnetism and the interpretation of anisotropy of magnetic susceptibility. Rev. Geophys. 30, 209–226.

Sagnotti, L., Sperenza, F., Winkler, A., Mattei, M., Funiciello, R., 1998. Magnetic fabric of clay sediments from the external northern Apennines (Italy). Phys. Earth Planet. Interiors 105, 73–93.

Saint-Bezar, B., 1999. Apport de la modélisation cinématique du plissement et de l'utilisation du magnétisme structurale à la compréhension d'un front de chevauchement aveugle: exemple du front sud atlasique, Goulmima (Maroc). PhD thesis, University of Cergy Pontoise.

Saint-Bezar, B., Frizon de Lamotte, D., Morel, J.L., Mercier, E., 1998. Kinematics of large-scale tip line folds from the High Atlas thrust belt, Morocco. J. Struct. Geol. 20, 999–1011.

Sans, M., Vergès, J., Gomis, J.M., Parès, J.M., Schiatarella, M., Travé, A., Doulcet, A., 1999. Layer parallel shortening in salt-detached folds: constraints on cross-section restoration. Thrust Tectonics 99, Royal Holloway University of London, 26–29 April 1999, Volume abstract, pp. 321–324.

Studer, M., 1980. Tectonique et pétrographie des roches sédimentaires, éruptives et métamorphiques de la région de Tounfit–Tirrhist (Haut–Atlas Central, Maroc). PhD Thesis University of Neuchâtel, Neuchâtel (Switzerland).

Suppe, J., 1983. Geometry and kinematics of fault-bend folding. Am. J. Sci. 283, 684–721.

Suppe, J., 1985. Principles of Structural Geology. Prentice-Hall Inc, Englewood Cliffs, NJ 537pp.

Suppe, J., Medwedeff, D.A., 1990. Geometry and kinematics of fault-propagation folding. Eclogae geol. Helvetica 83, 409–454.

Walker, T.R., 1967. Formation of red beds in modern and ancient deserts. Geol. Soc. Am. Bull. 78, 353–368.